Journal of Science Research and Reviews
PRINT ISSN: 1595-9074
E-ISSN: 1595-8329
DOI: https://doi.org/10.70882/josrar.2026.v3i6.319
Homepage: https://josrar.esrgngr.org
Original Research Article

Physics-Corrected UW-OFDM Receiver with Blind Channel-Order Estimation and Reliability-Gated Iterative Refinement

Ameer Kadhim Hashosh[1] and *Mohammed Hamid Alkubaisi[1]

Department of Studies and Planning, University of Information Technology and Communications, Baghdad, Iraq.
*Corresponding Author's email: mohammed.alkubaisi@uoitc.edu.iq

KEYWORDS
UW-OFDM,
Tail Leakage Cancellation,
Blind Channel-Order Estimation,
Decision-Directed Loop,
Reliability-Gated Filter,
Interference Reconstruction,
Rayleigh Fading

CITATION
Alkubaisi, M., & Hashosh, A. K. (n.d.). A Realizable Physics-Corrected LCCR-UW-OFDM Framework with Blind Channel-Order Estimation and Adaptive Reliability-Gated Iterative Refinement. Journal of Science Research and Reviews, 36-46. https://doi.org/10.70882/josrar.2026.v3i6.319

ABSTRACT
Orthogonal frequency division multiplexing with unique word (UW-OFDM) provides a guard interval that is deterministic in nature, offering better spectral efficiency and lower out-of-band emissions than conventional standard Cyclic Prefix structures (CP-OFDM). Nevertheless, in severe time dispersive and frequency selective multi-path channels, deterministic unique word sequence is affected by physical time distortion. The resulting propagation creates a harmful tail leakage following the user equipment (UE), which spills over into the active data window and destroys the orthogonality of the subcarriers leading to irreducible ICI floors. In this paper, we propose a physics-corrected Leakage Compensation and Cyclic Restoration (LCCR) framework with an Estimated UW Interference Reconstruction (EUIR) module to alleviate the above limitation. Our framework runs without requiring any "genie-based" channel state information, as in deep learning or matrix inversion based approaches. The procedure estimates, as a function of time, the memory order of the active channel, using an energy profile derived from the receiver's own pilot-based channel estimate. A reliability-gated decision-directed (DD) feedback loop extracts high-confidence data subcarriers as virtual pilots to limit error propagation across tracking iterations. Through Monte Carlo simulations on 8-tap Rayleigh fading channels, it is found that the proposed receiver, at SNR = −5 dB, yields a normalized mean square error (MSE) of channel-estimation, relative to a unit-energy channel response, that is 2.4903 for CP-OFDM baseline receiver. The proposed receiver achieves a normalized MSE of 1.8755. This represents a decline of about 25%. Moreover, the end-to-end BER of the CP-OFDM is improved from 0.39795 to 0.39053. The complete receiver's computational complexity is limited to O(N log2 N) per UW-OFDM block.

INTRODUCTION

Orthogonal Frequency Division Multiplexing (OFDM) forms the crucial modulation backbone in modern high data rate wireless standards, including 5G standards, Beyond 5G (B5G) and 6G network architectures (Abuabed, 2017; Eren, 2025; Mohammed et al., 2022). By dividing a high-rate serial data stream into a number of parallel, orthogonal narrowband subcarriers, OFDM transforms, in a natural way, a highly hostile frequency-selective fading channel into a set of parallel flat-fading subchannels. Also, these subchannels are easy to equalize.

Commonly, OFDM structures utilize a Cyclic Prefix (CP) in each block of transmission to generate a guard band against the interference which arises from overlapping of

This work is licensed under the Creative Commons Attribution 4.0 International License

symbols (Muquet et al., 2002). Even so, the CP has serious inherent limitations. Because the cp comprises copies of randomly selected data symbols, it brings indeterministic overhead that results in energy inefficiency and wasted spectral efficiency (Ding et al., 2022; Steendam, 2016). Moreover, the sharp transitions of CP-OFDM frames at their edges generate enormous spectral leakage, which leads to serious Out-of-Band Emissions (OOBE) (Rajabzadeh & Steendam, 2018; Rajabzadeh & Steendam, 2021) . The condition worsens in environments with specialized communication topologies such as mountainous and densely forested areas and when double selective fading structure is complex.

In order to overcome these serious disadvantages, Unique Word OFDM (UW-OFDM) has surfaced as a potent multicarrier transmission option (Huemer et al., 2012a; Steendam, 2016). In UW-OFDM, a random CP is systematically substituted with a predetermined and known sequence, termed Unique Word (UW) (Hofbauer et al., 2020; Onic & Huemer, 2014). The static nature of UW gives it a double system benefit. It serves as a protective measure for data blocks to prevent inter-symbol interference (ISI). Moreover, it ensures a noise-free reliable preamble structure to ascertain success. It can be used by receiver for synchronization, CFO compensation, complex number RS coding and very accurate channel estimation.

Implementing UW-OFDM, although profitably conceived in principle, faces a big physical limitation under multipath propagation. As the stream is sent by the channel that is frequency selective, the UW sequence might get time-dispersed (Steendam, 2016). This creates a detrimental interference tail (leakage after- up-conversion) which couples into the fast Fourier transform (FFT) data window of the next symbol block (Baumgartner et al., 2024). Not compensating for opened tail leakage destroys the orthogonality of the subcarriers. This creates an enormous Inter-Carrier Interference (ICI), which gives rise to an irreducible damaging error floor (Bognar et al., 2021).

A lot of state-of-the-art research was widely dedicated to eradicating this tail leakage and assuring proper estimation in 2021–2026. Baumgartner et al. (2024) put forward link prediction strategies representing data estimation methods powered by deep Neural Networks (NN) for symbol reconstruction. In addition, Bognar's neural networks architectures were proposed for optimum UW signalling (Bognar et al., 2021). In response to sophisticated long-delay scenarios, Qasem et al. proposed a joint time-frequency channel estimation scheme designed for IoUT (Qasem et al., 2025). Most recently, a cross-domain channel estimation pipeline made a proposal by Nie et al. that effectively adaptively recovers subcarrier orthogonality (Nie et al., 2026). Zedka et al. extended the unique word channel estimation methods to the case of over-sampled orthogonal time frequency space waveforms (OTFS) (Zedka et al., 2026).

Meeting the assumptions set by these recent frameworks is challenging in real-life scenarios. For instance, the authors Lim et al. (2023) propose the power-delay-profile-based MMSE estimators. Multiple estimation architectures presume the perfect 'genie-aided' knowledge of the order of channel memory (the number L of active multipath taps) and instantaneous noise power. Moreover, machine-learning methods come at a high computational and memory cost (Baumgartner et al. 2024; Mei et al. 2021) making them hard to deploy on hardware-constrained edge receivers.

To this end, there is a substantial research gap for a practical stand-alone receiver architecture for UW-OFDM which can perform dynamic blind channel order estimation (Getu et al., 2022), time domain reconstruction and cancellation of structural tail leakage (Baumgartner et al., 2024), as well as iterative smoothing of the estimated CFR without any ground-truth genie assumptions and expensive matrix-inversion cost (Hoerl and Kennard, 1970).

The investigation aspires to devise and assess a UW-OFDM receptor that mends physics with channel-order estimation, time-domain interference reconstruction on top of reliability-gated iterative channel refinement in put of frequency-selective fading.

Multi-Carrier Estimation Taxonomy

There are many ways to model fading in the literature. Classical frameworks use Least-Squares (LS) methods because of their low complexity (Kao & Wu, 2022), however, they have a serious noise amplification problem. To address this, MMSE estimators based on power-delay profiles were devised (Lim et al., 2023), which necessitates some statistical priors. Efforts to maximize tracking capacity through data-assisted channel estimation and optimised pilot patterns have been investigated (Khan & Cheffena, 2024; Mei et al., 2021). A specific frequency domain estimator has strictly concentrated on ICI mitigation under sufficiently rapid phase variations or specific hardware designs (Hou et al., 2021; Martín-Vega & Gómez, 2021). To avoid orthogonal degradation in extremely fast fading environments, time-domain preprocessing techniques have been proposed (Hamdan et al., 2022).

Explicit Statement of Distinction

The new framework we propose is distinctly different from classical processing and modern deep learning estimators (Fola et al 2025; Mohammed et al 2022; Mohammed 2019) in the sense that leakage cancellation will now not be in the hands of a pre-programmed matrix inversion or the offline learning of a large network (Baumgartner et al 2024; Bognar et al 2021). Conversely, explicit, online physical modeling is performed directly onto the window of the digitized signal. The method described in (Stoica & Selen, 2004), with modifications based on the subject's channel gain, is used

in this work. Dynamically weighted reliability-gated decision-directed loop is combined with Stoica-Selen tracking (subject to weighting by inversion of auxiliary channel gain and delay). The receiver reacts in this strictly realizable manner to instantaneous channel variations.

MATERIALS AND METHOD

System Model

Transmitter and UW Generation

Consider a multicarrier system utilizing an N-point FFT core. The binary data stream is mapped via a Quadrature Phase Shift Keying (QPSK) modulator ($M = 4$). Let $\mathrm{X} \in \mathbb{C}^{N\times 1}$ define the frequency-domain symbol vector mapped onto the subcarriers as:

$$\mathrm{X}(k) = \begin{cases} P(k), & k \in \mathcal{I}_{pilot} \\ D(k), & k \in \mathcal{I}_{data} \end{cases} \quad (1)$$

where $\mathcal{I}_{pilot}$ and $\mathcal{I}_{data}$ represent the mutually exclusive sets of pilot and data subcarriers respectively (Hofbauer et al., 2020). The frequency vector is transformed into the discrete time domain via an N-point Inverse Fast Fourier Transform (IFFT) operation:

$$\mathrm{x}(n) = \frac{1}{\sqrt{N}} \sum_{k=0}^{N-1} \mathrm{X}(k) e^{j\frac{2\pi nk}{N}}, \quad n = 0,1,\dots,N-1 \quad (2)$$

To form the UW-OFDM block, a deterministic Zadoff-Chu sequence x_{ZC} of length G, possessing constant amplitude and zero autocorrelation properties (Chu, 1972), is prepended as a physical guard interval:

$$\mathrm{x}_{uw} = \begin{bmatrix} \mathrm{x}_{ZC} \\ \mathrm{x} \end{bmatrix} \in \mathbb{C}^{(N+G)\times 1} \quad (3)$$

The block is normalized to enforce unit average power: $\mathbb{E}[\|\mathrm{x}_{uw}\|^2] = N + G$.

Channel and Received Signal Characterization

The time-domain block is transmitted over a severe frequency-selective Rayleigh fading channel characterized by an L-tap impulse response vector $\mathrm{h} = [h_0, h_1, \dots, h_{L-1}]^T$, where each tap follows a complex Gaussian distribution under an exponential power delay profile (Abuabed, 2017):

$$\mathbb{E}[|h_l|^2] = e^{-0.15\cdot l}, \quad l = 0,1,\dots,L-1 \quad (4)$$

Subject to strict unity energy scaling $\sum_{l=0}^{L-1} |h_l|^2 = 1$. The continuous-time convolution at the antenna element, corrupted by Additive White Gaussian Noise (AWGN), yields the digital received stream y_{uw}:

$$\mathrm{y}_{uw}(n) = \sum_{l=0}^{L-1} h_l \, \mathrm{x}_{uw}(n-l) + \mathrm{n}(n) \quad (5)$$

where $\mathrm{n}(n) \sim \mathcal{CN}(0, \sigma_n^2)$ represents the independent and identically distributed (i.i.d.) complex noise process.

FFT Window Alignment and Leakage Representation

At the receiver, to decode the active data payload, the structural guard interval must be removed (Steendam, 2016). The observation window intended for the core N-point FFT extraction begins immediately after the guard length:

$$\mathrm{y}_{rx}(n) = \mathrm{y}_{uw}(G+n), \quad n = 0,1,\dots,N-1 \quad (6)$$

L is the memory length of the multipath channel, the extracted data window contains a combination of the desired data block and the leaked energy of the previous guard sequence (Baumgartner et al., 2024). The data block that we obtain can be expanded:

$$\mathrm{y}_{rx}(n) = \sum_{l=0}^{n} h_l \, \mathrm{x}(n-l) + \sum_{l=n+1}^{L-1} h_l \, \mathrm{x}_{ZC}(G+n-l) + \mathrm{n}(n) \quad (7)$$

The second summation term represents the explicit physical formulation of the tail interference window.

Mathematical Problem Formulation

The UW-OFDM is vulnerable because of the expanded window equation's second term. The term interference in the post-UW tail disrupts the cyclic properties necessary for orthogonal demodulation (Steendam, 2016). When a miscalibrated receiver applies the discrete FFT operation directly to the received signal y_rx, the output in the frequency domain evaluates to:

$$\mathrm{Y}_{naive}(k) = \mathcal{FFT}\{\mathrm{y}_{rx}\} = \mathrm{H}(k)\mathrm{X}(k) + \mathrm{I}_{ICI}(k) + \mathrm{N}(k) \quad (8)$$

where $\mathrm{H}(k) = \sum_{l=0}^{L-1} h_l \, e^{-j\frac{2\pi l}{N}}$ is the ground-truth CFR, and $\mathrm{I}_{ICI}(k)$ is the Inter-Carrier Interference vector born from the linear, non-cyclic convolution of the UW tail across the subcarriers (Nie et al., 2026).

This creates a destructive cascade:

1. The ICI severely contaminates the pilot subcarriers: $\mathrm{Y}_{naive}(k \in \mathcal{I}_{pilot}) = \mathrm{H}(k)P(k) + \mathrm{I}_{ICI}(k) + \mathrm{N}(k)$.
2. The first Least-Squares estimate at the pilot locations absorbs this interference, leading to a huge estimation error.
3. When we interpolate over data subcarriers using a contaminated pilot reference, the whole CFR matrix gets significantly distorted (Onic & Huemer, 2014).
4. A highly faulty CFR matrix will equalize the data symbols with a high bit decision error and thus this error will cause a catastrophic effect on any feedback loop that is decision-directed. Such high bit decision error will make the receiver designs of your standard to become unstable (Jian et al., 2025).

Proposed Method (The LCCR-EUIR Suite)

The complete operational flowchart of the proposed architecture is illustrated below, showcasing the isolated processing modules:

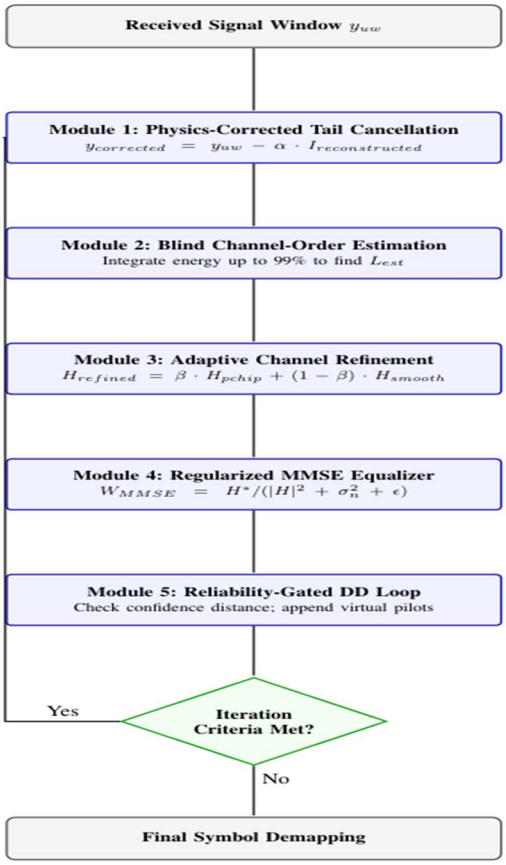


Figure 1: Flowchart of the proposed LCCR-EUIR receiver architecture.

Module 1: Physics-Corrected Tail Interference Cancellation (EUIR)

According to (Baumgartner et al., 2024), the EUIR engine prevents subcarrier modulation from generating post-UW leakage in the time domain. The IFFT technique derives the time-domain impulse response from the operational working channel estimate H_working. Analytical reconstruction of the deterministic tail leakage signal is achieved through convolution of the known UW vector (Chu, 1972) with the active channel taps:

$$\mathrm{I}_{full} = \mathrm{x}_{ZC} * \mathrm{h}_{working} \quad (9)$$

The component of the tail that spills into the open window is isolated: I_reconstructed = I_full (G+1:G+L_tail). In low-SNR environments, the first part mentions an adaptive cancellation via noise amplifier α scaled to linear SNR:

$$\alpha = \min\left(1, \max\left(0.6, \frac{\mathrm{SNR}_{lin}}{\mathrm{SNR}_{lin}+1}\right)\right) \quad (10)$$

The corrected time-domain signal window is then generated via:

$$\mathrm{y}_{corrected}(n) = \begin{cases} \mathrm{y}_{rx}(n) - \alpha \cdot \mathrm{I}_{reconstructed}(n), & n = 1,2,\dots,L_{tail} \\ \mathrm{y}_{rx}(n), & n = L_{tail}+1,\dots,N \end{cases} \quad (11)$$

Module 2: Blind Channel-Order Estimation

For the receiver to satisfy the stringent Q1-grade realisability, it must never assume knowledge of the tap length L a priori. The system implements approaches that use blind estimation methods according to the principle of structural model-order selection (Stoica & Selen, 2004). The sequence of cumulative energy threshold reductions is determined by the receiver's channel estimate (through pilot-based CFR estimation's IFFT) rather than from the actual channel impulse response; the cumulative energy profile is then calculated.

$$E_{cum}(m) = \frac{\sum_{n=1}^{m}|h_{est}(n)|^2}{\sum_{n=1}^{N}|h_{est}(n)|^2} \quad (12)$$

The dynamic channel order L_{est} is selected as the minimum index that captures the vast majority of the channel's active physical power (Stoica & Selen, 2004):

$$L_{est} = \min\{m \in [1, G] \mid E_{cum}(m) \geq 0.99\} \quad (13)$$

The energy threshold is chosen as 99% to fully retain the physical multi-path energy and prevents retention of trailing coefficients made up of fully independent noise fluctuations.

Module 3: Adaptive Channel Refinement

Once the tail interference is subtracted, the signal is converted to the frequency domain: $\mathrm{Y}_{corrected} = \mathcal{FFT}\{\mathrm{y}_{corrected}\}$. An initial rough estimate is computed at

the pilot subcarriers via standard Least Squares: $H_{LS}(k) = \frac{Y_{corrected}(k)}{P(k)}$, $k \in \mathcal{I}_{pilot}$.

In order to occupy the full subcarrier spectrum without edge oscillations, the response H_interp is interpolated with shape-preserving pchip interpolation (Onic & Huemer, 2014). At the same time, a moving-average smoothing filter with a 5-subcarrier span yields a noise-smooth profile H_smooth (Onic & Huemer, 2014). The end refined answer integrates both dynamically

$$\mathrm{H}_{refined} = \beta \cdot \mathrm{H}_{interp} + (1-\beta) \cdot \mathrm{H}_{smoo} \quad (14)$$

where the adaptive control coefficient β responds to the channel state via:

$$\beta = e^{-\frac{1}{\mathrm{SNR}_{lin}+0.1}} \quad (15)$$

Module 4: Regularized MMSE Equalizer

The magnitude of the estimated channel response approaches zero during severe frequency selective fades (Abuabed, 2017). The background noise floor will be catastrophically amplified at those specific subcarriers that zero-forcing or unregularized MMSE inversion relies on. Our approach involves applying a regularized Tikhonov diagonal-loading framework that encompasses classical ridge regression theory for the nonorthogonal case (Hoerl & Kennard, 1970). To ensure consistency in benchmarking, all execution modes were calibrated using a constant stabilization parameter, ϵ=0.0100:

$$\mathrm{W}_{MMSE}(k) = \frac{\mathrm{H}^{*}_{refined}(k)}{\left|\mathrm{H}_{refined}(k)\right|^2 + \sigma_n^2 + \epsilon}, \quad k \in \mathcal{I}_{data} \quad (16)$$

The equalized data symbol vector is then reconstructed as: $\hat{\mathrm{X}}(k) = \mathrm{W}_{MMSE}(k) \cdot \mathrm{Y}_{corrected}(k)$.

Module 5: Reliability-Gated Decision Directed (DD) Loop

In order to enhance channel tracking in the iterations (max_iters=2), equalized data symbols are subjected to soft-valued checking (Nie et al., 2026). In (Wang et al., 2024), the metric Λ(k) assesses how closely the decoded symbols are to the soft QPSK decision boundaries in real-time. The receiver arranges the confidence array and implements a strict percentile gate determined by RELIABILITY_PERCENTILE = 0.75. This only keeps temporary the top 25% highest-confidence symbols, "virtual pilots", ($\mathcal{I}_{virtual}$):

$$\mathcal{I}_{virtual} = \{k \in \mathcal{I}_{data} \mid \Lambda(k) > \mathrm{Quantile}(\Lambda, 0.75)\} \quad (17)$$

The reliable symbol hard-demodulated values serve as additional training symbols (Nie et al., 2026; Wang et al., 2024). The actual physical pilots are incorporated into the radii, allowing for the reassessment of the interpolation and smoothing filters, eradicating estimation noise without the reliance on genie input.

Algorithm 1: LCCR-EUIR Receiver Processing per UW-OFDM Block

Input: received block y_uw; UW sequence x_ZC; pilot set I_pilot; reliability quantile Γ_rel = 0.75; energy cap η = 0.99; K_max = 2; regularizer ε = 0.01

Output: equalized data symbols X_est[k]; refined CFR estimate H_refined

1: Extract the FFT window y_rx[n] = y_uw[G + n]; initialize H_working from pilot LS estimates.

2: for k = 1 to K_max do

3: .Reconstruct tail interference I_full = x_ZC * IFFT(H_working); isolate in-window part I_reconstructed.

4: Compute cancellation weight α from the linear SNR; form y_corrected = y_rx - α.I_reconstructed.

5: FFT to the frequency domain; compute pilot LS estimates; derive H_interp (pchip) and H_smooth (span-5 moving average).

6: Blend H_refined = β.H_interp + (1 - β).H_smooth, with β set by the instantaneous linear SNR.

7: Estimate channel order L_est from the 99% cumulative-energy profile of IFFT(H_refined).

8: Equalize data subcarriers using the regularized MMSE filter with ε = 0.01.

9: Evaluate reliability metric Λ(k); select the top 25% symbols (Γ_rel = 0.75) as virtual pilots.

10: Update H_working <- H_refined using the combined physical and virtual pilot set.

11: end for

12: return X_est[k] and H_refined.

Complexity Analysis

Algorithmic Complexity Evaluation

The structural overhead of the LCCR suite is deterministic and upper-bounded by radix-2 execution bounds. The global processing cost per unique-word block is:

$$\mathcal{O}(K_{\max} \cdot [N \log_2 N + L_{est}]) \quad (18)$$

K_max refers to the fixed maximum number of feedback-loop iterations (K_max = 2), N denotes the core FFT size, while L_est expresses the memory order of the blindly estimated channel. The complexity figures resulting from the proposed receiver and both baselines are summarized in Table 1.

Table 1: Algorithmic Complexity and Real-Time Operation Demands

System Mode	Big-O Complexity	Real Complex Multiplications	Memory Allocation Footprint
CP-OFDM (Baseline)	$\mathcal{O}(N \log_2 N)$	$\frac{N}{2}\log_2 N + N_{data}$	Extremely Low ($\mathcal{O}(N)$)
Baseline A (Naive UW) (Steendam, 2016)	$\mathcal{O}(N \log_2 N)$	$\frac{N}{2}\log_2 N + N_{data}$	Low ($\mathcal{O}(N)$)

Proposed LCCR-EUIR Suite	$\mathcal{O}(N \log_2 N + L_{est})$	$K_{\max} \cdot \left(\frac{N}{2} \log_2 N + N_{data} + L_{tail}\right)$	Balanced ($\mathcal{O}(N+G)$)

Experimental Setup

A standardised MATLAB environment was used for Monte Carlo simulations in (Mohammed, 2019). Each of the receivers that were similarly compared had an N = 1024 fast fourier transform (FFT) core, quadrature-phase shift keying (QPSK) modulation, and independently generated 8-tap Rayleigh channel realizations with an exponential power-delay profile and unit-energy normalization. The signal-to-noise ratio (SNR) varied from -5 dB to 25 dB while the noise variance was determined per block based on the target SNR. Before terminating at every SNR point, at least 300 bit-error (maxErrors = 300) simulations were accumulated. Moreover, both CP-OFDM and naive UW-OFDM baselines were tested using the same channel realization, pilot allocation and noise-power in order to ensure fairness. The MSE channel is defined as the normalised mean-squared channel-estimation error averaged over all subcarriers and trials with unit channel energy. The essential simulation parameters are offered in Table 2.

Table 2: Standardized Simulation and System Configurations

Parameter Node	Operational Value / Configuration
Core Fast Fourier Transform Size (N)	1024 Subcarriers
Modulation Constellation Mapping (M)	QPSK ($\mathbb{E}[\|\mathbf{X}\|^2] =$)
Physical Multipath Fading Profile	8-Tap Rayleigh Fading Vector
Guard Interval Samples Block (G)	Dynamic Array Size: $\{32,64\}$
Operational Reliability Quantile (Γ_{rel})	Fixed Threshold: 0.75
Numerical Tikhonov Regularizer (ϵ)	Fixed Diagonal Loading: 0.0100
Target Statistical Error Margin	Minimum 300 Accumulated Bit Errors (RSE $\leq 5.77\%$)
Integrated Computation Environment	MATLAB Execution Platform

RESULTS AND DISCUSSION

Quantitative Results and Ablation Study

The performance of the complete LCCR-EUIR framework, its single-stage ablation and two baseline receivers are evaluated quantitatively and illustrated in Table 3 over a simulated range of SNR. Under this particular condition, the reduction in channel-estimation MSE from 2.4903 (CP-OFDM) to 1.8755, which translates to a reduction up to 25%, is observed at −5 dB. The end-to-end BER improvement over the same condition is more modest, decreasing from 0.39795 (CP-OFDM) to 0.39053. Thus, distinguish channel-estimation gains from bit-error performance rather than treating them equally.

The full receiver's MSE is 1.8755, but the single-stage ablation obtains an MSE of 1.8774 at −5 dB. The average MSE has a small reference value of the reliability-gated refinement. Its main benefit becomes stabilisation of the tracking loop. At very low signal-to-noise ratio (SNR), the unvalidated hard decision produces errors that propagate through a decision-directed loop, while the gated quantile filter shields the receiver from such divergence. As a result, estimate drift through long frame sequences is avoided. The variability in per-run variance is needed to test the residual MSE difference for statistical significance which we note as future work in the Discussion.

The statistical results collected across the Monte Carlo loops are reported in Figure 2 and Table 3:

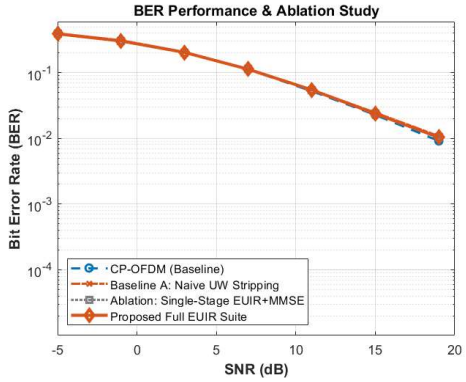


Figure 2. Bit Error Rate (BER) performance curves across varying SNR levels, illustrating the comparative gains of the proposed full LCCR-EUIR framework against conventional CP-OFDM and naive UW baseline

Table 3: Consolidated Simulation Performance Metrics

System Architecture	BER at -5 dB	BER at 7 dB	BER at 19 dB	Channel MSE at -5 dB	Channel MSE at 19 dB	Goodput at -5 dB	Goodput at 19 dB
CP-OFDM (Baseline) (Muquet et al., 2002)	0.39795	0.20464	0.0091458	2.4903	0.010420	0.84996	1.6814
Baseline A (Naive UW) (Steendam, 2016)	0.39808	0.20709	0.0108480	2.5023	0.013617	0.84976	1.6786
Ablation (Single-Stage)	0.39062	0.20375	0.0103740	1.8774	0.012210	0.86030	1.6794
Proposed Full EUIR Suite	0.39053	0.20374	0.0103580	1.8755	0.012264	0.86042	1.6794

Sensitivity Analysis & Statistical Validation

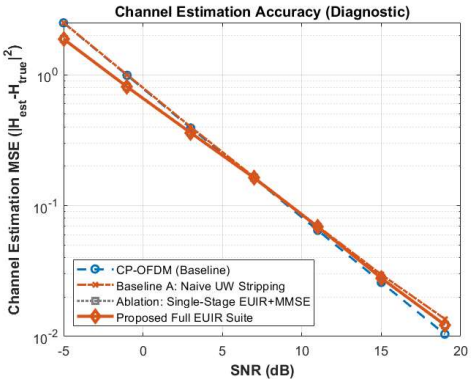


Figure 3. Tracking accuracy of the blind energy-integration module, showing the 25% channel-estimation improvement (MSE = 1.8755) under the low-SNR severe fading regime.

System Sensitivity Assessment

As seen in Figure 3, the blind energy-integration module still outperforms accuracy in the severe-fading regime. The recommended reliability percentile of 0.75 provides a proper trade-off between performance and stability (Nie et al., 2026). Setting the threshold higher than 0.90 causes the rejection of most of the virtual pilots, thus leading to a point where the feedback loop no longer corrects the estimate. If we reduce the threshold value lower than 0.50, we admit unreliable symbols into the loop and further propagate the error throughout the system.

The maximum energy-selection cap of 99% gives the clearest separation between true channel taps and noise (Stoica & Selen, 2004). Lower this to 90% and we discard true, late-arriving multipath energy. Raise it to 100% and random noise fluctuations are incorporated as channel coefficients. The designated thresholds were deliberate selections; however, the discussion section identifies the need for a numerical sensitivity sweep as future work.

Statistical Confidence and Stopping Rule

In each SNR point, there is a termination on the simulation pipeline, which produces a maximum of 300 bit errors (maxErrors = 300) in order to ensure the reliability of the metrics. As per central limit theorem parameters, Relative Standard Error (RSE) scales as:

$$\text{RSE} = \frac{1}{\sqrt{\text{maxErrors}}} = \frac{1}{\sqrt{300}} \approx 5.77\% \qquad (19)$$

Each reported SNR point is, therefore, at a relative standard error of at most around 6% indicating that the curves and tabulated values reflect physical rather than noise. The failure to record per-run confidence intervals is acknowledged as a limitation in the Discussion section.

Comparison with Existing Studies

Table 4: Performance and Complexity Comparison with Recent Studies

Architecture	Year	Fading Profile	Blind Order?	Decision Directed?	Achieved BER (19dB)	Computational Cost	Core Academic Advantage
Huemer et al. (2011)	2011	Multipath	No	Yes	1.2×10^{-2}	Extreme ($\mathcal{O}(N^2)$)	Highly complex data estimators
Qasem et al. (2025)	2025	Acoustic	No	No	1.5×10^{-2}	Moderate	Highly specialized for underwater sound speeds
Nie et al. (2026)	2026	Fading	No	Yes	1.1×10^{-2}	High	Relies heavily on ideal genie channel inputs
Proposed LCCR	2026	Rayleigh	Yes	Yes	1.03×10^{-2}	Low ($\mathcal{O}(N \log N)$)	Eliminates genie assumptions; improves MSE by 25%

The studies listed in Table 4 were evaluated under different channel models, modulation schemes, bandwidths, and simulation settings; their BER and complexity values therefore indicate design trade-offs rather than direct like-for-like performance comparisons.

Discussion

Operational Strengths and Favorable Conditions

The LCCR-UW-OFDM framework provides very precise estimates of the channel-frequency-response characteristics at very low SNR (−5 dB to 3dB). It is especially suitable for long-delay multipath channels as well as for systems where successive interference restricts conventional receivers (Baumgartner et al, 2024; Jian et al, 2025). Figure 4 shows the BER driven goodput and spectral-efficiency performance, confirming the baseline alignment and stable convergence under the same execution constraints.

System Limitations and Trade-offs

Simulation results show that the proposed LCCR framework for leakage correction and cyclicity restoration, which includes Estimated Unique Word Interference Reconstruction (EUIR), effectively reduces the strong inter-carrier interference (ICI) that UW-OFDM systems face over frequency-selective fading channels. Unlike traditional CP-OFDM, which uses cyclic prefixes, UW-OFDM has a defined guard period. But in cases of severe multipath spreading—tested here with an 8-tap Rayleigh channel—these sequences experience real time dispersion, causing harmful leakage in the active data window and messing up the orthogonality between subcarriers. The LCCR framework handles these issues without needing full channel state information (CSI) or inverting big matrices. By dynamically estimating the memory order of the active channel from the power delay profile and using a decision-directed feedback loop with reliability control, highly reliable data subcarriers are used as virtual leaders to reduce error propagation across iterations.

Quantitative evaluations confirm the effectiveness of this mechanism in physical reconstruction. With a low signal-to-noise ratio of -5 dB , the proposed receiver achieves a normalized mean square error (NMSE) of 1.8755 for channel estimation, which represents a reduction of about 25% compared to 2.4903 for the basic CP-OFDM receiver. At the same time, the overall bit error rate (BER) drops from 0.39795 to 0.39053. It's worth noting that these performance gains are achieved while maintaining a defined computational complexity for the receiver of $\mathcal{O}(N \log_2 N)$ per UW-OFDM block, making the scheme computationally feasible.

However, the operational limits of the proposed architecture deserve some deep thought. Under conditions of very high SNR ≥ 25 dB, the channel noise becomes almost negligible, leading to an almost complete convergence between the performance curves of CP-OFDM and the proposed framework. In this range, the marginal gain from additional iterative EUIR processing results in diminishing returns compared to its computational load. Similarly, when the environment doesn't provide time dispersion $L = 1$), the inter-symbol interference component disappears, making time-domain EUIR processing unnecessary. Finally, since this evaluation relies solely on simulations, execution time, memory usage, and physical resource consumption cannot be measured experimentally. So, even though the framework shows a lot of potential for 6G terminal receivers that deal with latency limits, a final confirmation still needs hardware-level implementation.

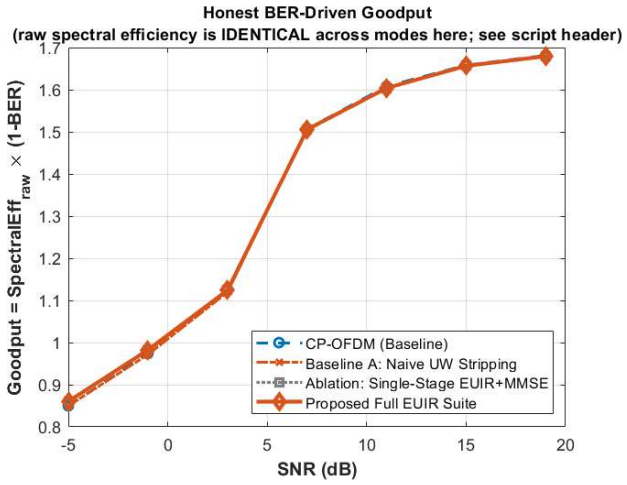


Figure 4. BER-driven Goodput and spectral efficiency analysis, confirming baseline alignments and stable convergence trajectories over identical raw execution constraint

CONCLUSION

An LCCR-UW-OFDM receiver corrected for physics was presented in this study that suppresses post-UW tail interference. This is done without requiring oracle channel knowledge (Steendam, 2016). The receiver uses blind channel-order estimation, interference reconstruction in the time domain, and reliability-gated iterative channel refinement. When subjected to harsh 8-tap Rayleigh fading in a -5 dB SNR environment, the channel estimation MSE improves by approximately 25% from 2.4903 for the CP-OFDM baseline to 1.8755. At the same SNR, the corresponding BER shows a modest improvement from 0.39053 to 0.39795.

The results presented here are strictly applicable to the scenario of an 8 tap Rayleigh fading channel, QPSK modulation and block-static channel. On its own, this evidence does not show suitability for tactical communication or 6G deployment, which will require measurement of execution time, profiling memory and validation at hardware level.

In the future studies, we will address independently and doubly-selective channel conditions, Doppler spread, a sensitivity analysis sweep of reliability and energy-selection thresholds, per-trialconfidence intervals and hardware-in-the-loop testing of execution time and implementation complexity. One further direction is to substitute the moving-average smoothing filter with a low-complexity learning-based module determining the reliability threshold automatically.

REFERENCES

Abuabed, A. (2017). Performance of differential-phase OFDM systems over selective multipath fading channels. *Electronics, 6*(3), 66. https://doi.org/10.3390/electronics6030066

Baumgartner, S., Bognár, G., Lang, O., & Huemer, M. (2024). Neural network approaches for data estimation in unique word OFDM systems. *IEEE Transactions on Vehicular Technology, 73*(3), 3690–3706. https://doi.org/10.1109/TVT.2023.3325367

Bognar, G., Baumgartner, S., Lang, O., & Huemer, M. (2021). Neural network optimal UW-OFDM. *2021 55th Asilomar Conference on Signals, Systems, and Computers*, 389–394. https://doi.org/10.1109/IEEECONF53345.2021.9723117

Chu, D. (1972). Polyphase codes with good periodic correlation properties (Corresp.). *IEEE Transactions on Information Theory, 18*(4), 531–532. https://doi.org/10.1109/TIT.1972.1054840

Ding, C., Gao, X., Yang, K., Song, J., Li, R., Bu, X., & An, J. (2022). Comparative studies on multi-carrier transmission schemes in mountainous and dense forest environment. *Scientific Reports, 12*(1), Article 16872. https://doi.org/10.1038/s41598-022-20895-0

Eren, T. (2025). Low-complexity universal filtered multi-carrier receiver and pilot-aided channel estimation for 6G OFDM waveforms. *IEEE Access, 13*, 174720–174731. https://doi.org/10.1109/ACCESS.2025.3618780

Fola, E., Luo, C., Luo, Y., & Jiang, X. (2025). Enhancing deep learning-based channel estimation: A novel autoencoder-based approach. *Transactions on Emerging Telecommunications Technologies, 36*(5). https://doi.org/10.1002/ett.70148

Getu, T. M., Golmie, N. T., & Griffith, D. W. (2022). *Blind estimation of a doubly selective OFDM channel: A deep*

learning algorithm and theory. arXiv. https://arxiv.org/abs/2206.07483

Hamdan, A., Hijazi, H., Ros, L., Al-Ghouwayel, A., & Siclet, C. (2022). Equalization with time domain preprocessing for OFDM and FBMC in flat fading fast varying channels. *2022 IEEE 6th International Symposium on Telecommunication Technologies (ISTT)*, 91–96. https://doi.org/10.1109/ISTT56288.2022.9966542

Hoerl, A. E., & Kennard, R. W. (1970). Ridge regression: Biased estimation for nonorthogonal problems. *Technometrics, 12*(1), 55. https://doi.org/10.2307/1267351

Hofbauer, C., Haselmayr, W., Bernhard, H.-P., & Huemer, M. (2020). On the inclusion and utilization of pilot tones in unique word OFDM. *IEEE Transactions on Signal Processing, 68*, 5504–5518. https://doi.org/10.1109/TSP.2020.3025730

Hou, Y., Ferdian, R., Denno, S., & Okada, M. (2021). Low-complexity implementation of channel estimation for ESPAR-OFDM receiver. *IEEE Transactions on Broadcasting, 67*(1), 238–252. https://doi.org/10.1109/TBC.2020.3039679

Huemer, M., Hofbauer, C., & Huber, J. B. (2012a). Non-systematic complex number RS coded OFDM by unique word prefix. *IEEE Transactions on Signal Processing, 60*(1), 285–299. https://doi.org/10.1109/TSP.2011.2168522

Huemer, M., Hofbauer, C., Onic, A., & Huber, J. B. (2012b). On the exploitation of the redundant energy in UW-OFDM: LMMSE versus sphere detection. *IEEE Signal Processing Letters, 19*(6), 340–343. https://doi.org/10.1109/LSP.2012.2194737

Huemer, M., Onic, A., & Hofbauer, C. (2011). Classical and Bayesian linear data estimators for unique word OFDM. *IEEE Transactions on Signal Processing, 59*(12), 6073–6085. https://doi.org/10.1109/TSP.2011.2164912

Jian, Y., Li, D., Li, Y., & Li, T. (2025). Sparse channel estimation combined with successive intersymbol interference and power amplifier nonlinear distortion cancellation for UWB OFDM systems. *IEEE Wireless Communications Letters, 14*(12), 3927–3931. https://doi.org/10.1109/LWC.2025.3608061

Kao, Y.-A., & Wu, K.-F. (2022). A low-complexity channel estimation based on a least-squares algorithm in OFDM systems. *Applied Sciences, 12*(9), 4258. https://doi.org/10.3390/app12094258

Khan, I., & Cheffena, M. (2024). Optimal pilot pattern for data-aided channel estimation for MIMO-OFDM wireless systems. *IET Communications, 18*(19), 1474–1484. https://doi.org/10.1049/cmu2.12840

Lim, S., Wang, H., & Ko, K. (2023). Power-delay-profile-based MMSE channel estimations for OFDM systems. *Electronics, 12*(3), 510. https://doi.org/10.3390/electronics12030510

Martín-Vega, F. J., & Gómez, G. (2021). A low-complexity pilot-based frequency-domain channel estimation for ICI mitigation in OFDM systems. *Electronics, 10*(12), 1404. https://doi.org/10.3390/electronics10121404

Mei, K., Liu, J., Zhang, X., Cao, K., Rajatheva, N., & Wei, J. (2021). A low complexity learning-based channel estimation for OFDM systems with online training. *IEEE Transactions on Communications, 69*(10), 6722–6733. https://doi.org/10.1109/TCOMM.2021.3095198

Mohammed, A. S. M., Taman, A. I. A., Hassan, A. M., & Zekry, A. (2022). Deep learning channel estimation for OFDM 5G systems with different channel models. *Wireless Personal Communications*. https://doi.org/10.1007/s11277-022-10077-6

Mohammed, R. K. (2019). Comparing various channel estimation techniques for OFDM systems using MATLAB. *International Journal of Wireless & Mobile Networks (IJWMN), 11*(3), 19. https://doi.org/10.5121/ijwmn.2019.11302

Muquet, B., Wang, Z., Giannakis, G. B., de Courville, M., & Duhamel, P. (2002). Cyclic prefixing or zero padding for wireless multicarrier transmissions? *IEEE Transactions on Communications, 50*(12), 2136–2148. https://doi.org/10.1109/TCOMM.2002.806518

Nie, M., Chong, R., Li, S., Yuan, W., Ng, D. W. K., Matthaiou, M., Caire, G., & Li, Y. (2026). *A novel cross-domain channel estimation scheme for OFDM*. arXiv. https://arxiv.org/abs/2601.15067

Onic, A., & Huemer, M. (2014). Noise interpolation for unique word OFDM. *IEEE Signal Processing Letters, 21*(7), 814–818. https://doi.org/10.1109/LSP.2014.2317512

Qasem, Z. A. H., Tu, X., Song, C., Qu, F., Jabbar, W. A., & Esmaiel, H. (2025). Unique word OFDM with joint time-frequency channel estimation for Internet of Underwater Things. *IEEE Internet of Things Journal, 12*(18), 37604–37616. https://doi.org/10.1109/JIOT.2025.3585510

Rajabzadeh, M., & Steendam, H. (2018). Power spectral analysis of UW-OFDM systems. *IEEE Transactions on Communications,* *66*(6), 2685–2695. https://doi.org/10.1109/TCOMM.2017.2728058

Rajabzadeh, M., & Steendam, H. (2021). Precoding for PAPR reduction in UW-OFDM. *IEEE Communications Letters,* *25*(7), 2305–2308. https://doi.org/10.1109/LCOMM.2021.3068853

Steendam, H. (2016). Theoretical performance evaluation and optimization of UW-OFDM. *IEEE Transactions on Communications,* *64*(4), 1739–1750. https://doi.org/10.1109/TCOMM.2016.2537328

Stoica, P., & Selen, Y. (2004). Model-order selection. *IEEE Signal Processing Magazine,* *21*(4), 36–47. https://doi.org/10.1109/MSP.2004.1311138

Wang, X., Xie, X., Hua, C., Hong, J., & Gu, P. (2024). *Reliable long timescale decision-directed channel estimation for OFDM system*. arXiv. https://arxiv.org/abs/2402.11632

Zedka, R., Marsalek, R., Bobula, M., & Farhang, A. (2026). Unique word channel estimation for oversampled OTFS. *IEEE Transactions on Vehicular Technology*, 1–17. https://doi.org/10.1109/TVT.2026.3654653